



How the presence of a giant planet affects the outcome of terrestrial planet formation simulations

Zhihui Kong^{1,2} , Anders Johansen^{2,4} , Michiel Lambrechts², Jonathan H. Jiang³, and Zong-Hong Zhu¹

¹ Department of Astronomy, Beijing Normal University, Beijing, PR China
e-mail: 201831160004@mail.bnu.edu.cn

² Center for Star and Planet Formation, Globe Institute, University of Copenhagen, Øster Voldgade 5–7, 1350 Copenhagen, Denmark

³ Jet Propulsion Laboratory, California Institute of Technology, Pasadena, USA
e-mail: Jonathan.H.Jiang@jpl.nasa.gov

⁴ Lund Observatory, Department of Astronomy and Theoretical Physics, Lund University, Box 43, 221 00 Lund, Sweden

Received 20 December 2023 / Accepted 7 May 2024

ABSTRACT

The architecture and masses of planetary systems in the habitable zone could be strongly influenced by the presence of outer giant planets. Here, we investigate the impact of outer giants on terrestrial planet formation, under the assumption that the final assembly of the planetary system is set by a giant impact phase. Utilizing a state-of-the-art N -body simulation software, GENGA, we interpret how the late stage of terrestrial planet formation contributes to diversity among planetary systems. We designed two global model setups: 1) we placed a gas giant on the outer side of planetesimals and embryo disk and 2) we only included planetesimals and embryos, but no giant. For the model including the outer giant, we studied the effect of different giant initial masses in the range of 1.0–3.0 Jupiter masses, as well as a range of orbital radii from 2.0–5.8 AU. We also studied the influence of different initial positions of planetesimals and embryos on the results. Our N -body simulation time is approximately 50 Myr. The results show that the existence of an outer giant will promote the interaction between planetesimals and embryos, making the orbits of the formed terrestrial planets more compact. However, placing the giant planet too close to the planetesimals and embryo disk suppresses the formation of massive rocky planets. In addition, under the classical theory, where planetary embryos and planetesimals collide to form terrestrial planets, our results show that the presence of a giant planet actually decreases the gap complexity of the inner planetary system.

Key words. planets and satellites: dynamical evolution and stability – planets and satellites: formation – planets and satellites: terrestrial planets – protoplanetary disks – planetary systems

1. Introduction

Over the past three decades, exoplanet researchers have discovered more than five thousand planets outside our Solar System (Winn & Fabrycky 2015). We have witnessed a huge diversity in the exoplanet population, which is reflected in many types of planets discovered, such as super-Earths, hot gas giants, cold gas giants, ice giants, and terrestrial planets. The orbits and eccentricities of planets in multiple systems provide another window into exoplanetary systems (Lissauer et al. 2011; Weiss et al. 2018). This motivates us to generalize terrestrial planet formation models to account for the diversity seen among exoplanet systems.

According to the standard model, planet formation can be divided into three stages: 1) growth from dust to pebbles by coagulation, 2) assembly of planetesimals from pebbles, 3) and growth to embryos and fully formed planets by mutual impacts, pebble accretion, and gas accretion (Raymond et al. 2004, 2006a; Levison et al. 2010; Johansen et al. 2015; Levison et al. 2015; Mordasini et al. 2015; Wurm 2018; Johansen et al. 2021). The focus of this article is the stage of terrestrial planet formation via impacts, specifically addressing the process by which planetary embryos grow into terrestrial planets. In the classical model, terrestrial planets form through a series of violent collisions among numerous planetary embryos and planetesimals (Wetherill 1990; Chambers 1999). Several studies show that this process requires approximately 30–100 Myr for Earth to form

(Chambers 2001; John et al. 2010; Raymond et al. 2014). Nevertheless, when pebble accretion is taken into account, the Earth can form much faster within the protoplanetary disc, namely, in 3–5 Myr (Liu & Ormel 2018; Lambrechts et al. 2019; Brož et al. 2021; Johansen et al. 2021). Gas giants must form rapidly within the protoplanetary disc under all circumstances. However, analyses of numerous star clusters of different ages indicate that the typical timescale for the protoplanetary disc is only a few Myr, which is earlier than the inner terrestrial planet formation stage (Chambers & Wetherill 1998; Haisch et al. 2001; Briceño et al. 2001; Hillenbrand et al. 2008; Hasegawa & Pudritz 2012; Nesvorný et al. 2021). Therefore, the presence of giant planets must significantly influence the process of terrestrial planet formation. In this paper, we explore the formation of terrestrial planets by giant impacts after the dissipation of the protoplanetary disc. We critically compare two models: one incorporates an external gas giant in the formation of terrestrial planets, while the other excludes the presence of any giants. In this way, we can investigate the role of gas giant planets in the shaping the masses and orbits of inner terrestrial planet systems.

Furthermore, N -body simulation methods have proven to be highly valuable for understanding the orbital patterns of Earth-like planets within our Solar System, such as the differences and similarities between Venus and Earth and between Earth and Mars (Raymond et al. 2004; Hansen 2009; Nesvorný et al. 2021; Woo et al. 2022; Batygin & Morbidelli 2023). Meanwhile, several studies have not only explored the planetary architecture

within our Solar System, but also the growth of rocky planets during giant planet instabilities, aiming to explain the diversity of exoplanets (Raymond et al. 2011, 2012; Carrera et al. 2015). In this paper, we explore the presence of a giant planet as a free parameter in terrestrial planet formation, with a mass range of 1–3 Jupiter mass and an orbital range between 2–5.8 AU. Nesvorný et al. (2021) investigated the impact of a giant planet instability on the formation of terrestrial planets and found that accelerates the growth of the terrestrial planets. This implies that the instability of giant planets likely occurred during the process of terrestrial planet formation (Clement et al. 2018, 2019). The authors examine various instability scenarios previously found to align with numerous Solar System constraints. They discovered that resonances with giant planets contribute to the removal of solids available for accretion near 1.5 AU, thereby impeding the growth of Mars. These authors, taking a view centered on the Solar System, used their N -body simulation to match the structure of terrestrial planets in the Solar System. In addition, some works have focused on how a migrating chain of giant planets affects the terrestrial planets formation (Fogg & Nelson 2005, 2007; Raymond et al. 2006b; Thommes et al. 2008). In our study, however, we conducted a multitude of N -body simulations to explore the structural diversity of exoplanet systems and elucidate the impact of outer gas giants on the variety observed in inner terrestrial planetary systems.

In addition, CPU-based N -body simulation codes have served as the primary tool for investigating planet formation; however, due to computational constraints, planetesimals in these simulations are usually treated as test particles that can only interact with and experience the gravitational force from more massive embryos; however, they cannot mutually interact with each other (O’Brien et al. 2006; Walsh & Morbidelli 2011; Jacobson & Morbidelli 2014; Brasser et al. 2016; Quintana et al. 2016). This approximation can significantly lower the total number of active particles in the system and keep the computational time reasonable. However, such simplified simulation settings could lead to strong limitations in fully understanding the process of terrestrial planet formation, especially for modeling the growth of Mars. Woo et al. (2022) used GPU-based algorithms to conduct simulations over extended time periods in systems comprising a substantial number of particles. In our study, we use the *GENGA* code by Grimm & Stadel (2014) to accelerate the simulation process. We carried out a comprehensive analysis using a total of 140 simulation samples, wherein we systematically varied the initial state of the gas giant. Each sample simulation time is about 50 Myr, which basically covers the evolution process from the planetary embryo to the protoplanet.

In the study by He & Weiss (2023), the *Kepler* Giant Planet Search (KGPS), as detailed by Weiss et al. (2024), was employed to investigate the influence of outer gas giants on the masses and orbits of inner, smaller planets. The findings indicate that systems with an outer giant planet exhibit a higher level of gap complexity. Following that approach, we applied a comparable methodology to analyze our simulation samples. We do not include the effects of the gas giant formation phase and its early migration on the velocity dispersion of the planetesimals in the inner regions of the disc, although these are potentially important (Walsh & Morbidelli 2011; Guo & Kokubo 2023). These aspects will be the focus of our future research.

We outline this paper as follows. In Sect. 2, we introduce the numerical method and describe the inner disk of planetesimals and embryos and the orbital parameters of the outer gas giant. In Sect. 3, we present the results of the N -body simulations. We investigate the impact of initial states of giant planets

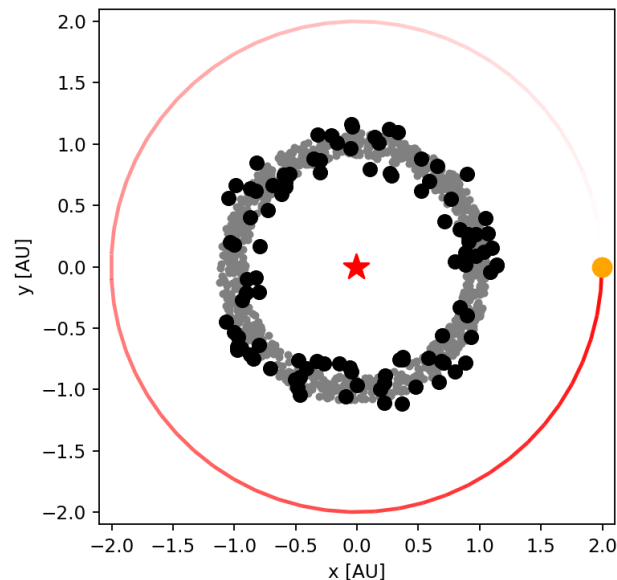


Fig. 1. Simulation setup using the REBOUND code, featuring a central star with a solar mass. Orbiting the star are 100 planetary embryos, each with a mass of 0.05 Earth masses (represented by black dots) and 1000 planetesimals, each with a mass of 0.005 Earth masses (represented by gray dots), arranged in a ring approximately 1 AU in radius. Additionally, a gas giant (represented by an orange dot) orbits at a distance of 2 AU.

on the formation of terrestrial planets and present our findings in Sect. 3.1. We describe the concept of gap complexity in Sect. 3.2. A statistical analysis is performed on the simulation samples in Sect. 3.3. In Sect. 4, we present a comprehensive summary of the simulation results for three distinct types of samples representing the final stage of terrestrial planet formation in Sect. 4.1. We succinctly outline the limitations of our model and provide a forward-looking perspective on potential avenues for future research endeavors in Sect. 4.2.

2. Method

In this section, describe how we construct a 3D global N -body simulation model based on classical terrestrial planet formation model to investigate the influence of outer giants on the terrestrial planet formation. We focused on the study of collisions between planetesimals and planetary embryos, while disregarding the migration of the giant planet.

2.1. Introducing the N -body codes

The N -body simulation software *REBOUND*, extensively employed in the field of astrophysics, contains both a non-symplectic integrator, with adaptive time stepping (Everhart 1985; Rein & Liu 2012; Rein & Spiegel 2015) and a hybrid symplectic integrator (Rein et al. 2019), that is similar to the *MERCURY* (Chambers 1999). Consequently, *REBOUND* has evolved into a pivotal research tool for investigating planet formation and orbital dynamics (Lam & Kipping 2018; Kong et al. 2022). It is straightforward to set up a model with this code, such as Fig. 1 that illustrates a planetary system comprising a solar mass, 100 planetary embryos, and 1000 planetesimals positioned at approximately 1 AU, and accompanied by a gas giant-sized placed in an exterior orbit. However, the *REBOUND* code, which utilizes the CPU as the fundamental arithmetic unit,

Table 1. Model parameters.

Mass of the central star	$1 M_{\odot}$
Total mass of embryos	$5 M_{\oplus}$
Total mass of planetesimals	$5 M_{\oplus}$
Number of embryos	100
Number of planetesimals	1000
Orbits of embryos	0.8 – 1.2 AU
Orbits of planetesimals	0.9 – 1.1 AU
Calculation step	6 days
Total time	≈ 50 Myr

exhibits suboptimal performance in long-term simulations of high particle numbers. This is true despite the fact that it also provides a parallel computing scheme.

Leveraging the GPU as the fundamental computational unit in *GENGA*, the inherent parallel computing logic facilitates enhanced computational speed, rendering it an efficient tool for investigating the last stage of terrestrial planets formation by numerous collisions between planetary embryos and planetesimals. Moreover, *GENGA* enables simulation over extended duration. However, constructing a model using this code necessitates inputting the position and velocity data for each individual particle, which proves inconvenient when dealing with models comprising a substantial number of particles. Hence, in this study, we initially employ *REBOUND* to set up a range of planetary systems with diverse initial conditions, evolving the model parameters in the requisite *GENGA* format for subsequent extensive simulations.

2.2. Model setup

Previous research has shown that a narrow annulus of planetesimals and embryos is conducive to the formation of Earth-mass terrestrial planets (Hansen 2009; Kaib & Cowan 2015; Raymond & Izidoro 2017; Nesvorný et al. 2021; Izidoro et al. 2021; Joiret et al. 2023). Therefore, we designed two models, one with a giant planet on the outside of the disk, and one with no giant. We set the central star to 1 solar mass and uniformly place 100 planetary embryos of $0.05 M_{\oplus}$ between 0.8 and 1.2 AU, for a total mass of $5 M_{\oplus}$, and uniformly placed 1000 planetesimals of $0.005 M_{\oplus}$ between 0.9 and 1.1 AU, for a total additional mass of $5 M_{\oplus}$. The eccentricity of embryos and planetesimal were set according to a Rayleigh distribution with mean value of 0.01, while their inclinations were set as a Rayleigh distribution with a mean value of 0.005. Here, the Rayleigh distribution is given as function with mean sigma, defined as $\text{Rayleigh}(\sigma) = \sigma \sqrt{-2 \ln(\text{uniform}[0, 1])}$ where $\text{uniform}[0, 1)$ represents a uniformly distributed random variable between 0 and 1 (with 1 excluded). We note that by using a distribution of inclinations, we are considering a 3D model rather than a plane.

Next, we transfer the initial model into the *GENGA* code for a simulation time of about 50 Myr. In practice, the calculation step is six days and the total number of simulation steps is 3×10^9 . This yields a total simulation time of approximately 50 Myr and the file recording interval is about 0.1 Myr. To improve the running speed, the storage interval for the first 10 Myr is set at 0.1 Myr, and for the subsequent 40 Myr, it is changed to 1 Myr. The model parameters are summarized in Table 1, while the parameters for the outer gas giants are presented in the subsequent section (Sect. 2.3). In this study, planetesimals and embryos are mixed and placed in a narrow

Table 2. Naming convention.

Group name	Included samples	Mass of giant	Orbit of giant
No giant	nogiant_000-020		
With giant	giant_001-020	$1.0 M_{\text{Jup}}$	2 – 5.8 AU
	giant_021-040	$1.5 M_{\text{Jup}}$	2–5.8 AU
	giant_041-060	$2.0 M_{\text{Jup}}$	2–5.8 AU
	giant_061-080	$2.5 M_{\text{Jup}}$	2–5.8 AU
	giant_081-100	$3.0 M_{\text{Jup}}$	2–5.8 AU
	clone_001-020	$2.0 M_{\text{Jup}}$	3.2 AU

annulus, with all particles in the model acting as active particles. When two particles come into close proximity, they undergo collision and either merge or experience a scattering event. We run *GENGA* with its default a collision condition. The resolution in terms of particle number is comparable to the first “high-resolution” simulations of terrestrial planet formation (Raymond et al. 2006a; O’Brien et al. 2006; Morishima et al. 2008), but lower than many current simulations. However, we established 140 simulated samples to study the influence of outer giants on the formation of inner terrestrial planets. The parameters for giant stars are set in Sect. 2.3.

2.3. Configuration of gas giants

We categorized our samples into two groups: the “no giant” group represents scenarios where only planetesimals and embryos are present, without the inclusion of a gas giant in the outer system. The initial states of planetesimals and planetary embryos are randomly generated based on their distribution as discussed in Sect. 2.2. In the “with giant” group, we investigate the influence of an outer gas giant on the formation of terrestrial planets within a mass range of 1.0–3.0 Jupiter masses with intervals of $0.5 M_{\text{Jup}}$, and orbits ranging from 2.0 to 5.8 AU with intervals of 0.2 AU. In addition, the eccentricity of the gas giant is set to 0.05, since the resulting gravitational perturbations can quantitatively affect the outcome of terrestrial planet accumulation (Chambers 2001; O’Brien et al. 2006). Moreover, in our model, the giant is influenced by the inner disk, which can lead to changes in eccentricity over time as illustrated in Fig. 2. Much previous work has noted this phenomenon (Chambers & Wetherill 1998; Chambers 2001; Raymond et al. 2004, 2006a; Brasser et al. 2023) and here we quantify it in Sect. 3.3. Meanwhile, we maintain the same initial state for planetesimal and planetary embryos in each sample. We established an additional set of samples, which we name clone_001-020, to investigate the impact of the randomized initial states of planetesimals and planetary embryos on the outcome of terrestrial planet formation. In the clone_001-020 samples, we take the same initial state of a gas giant as giant_047 (with a giant planet mass of $2.0 M_{\text{Jup}}$ orbiting at 3.2 AU) and randomly generate planetesimals and embryos based on the distribution outlined in Sect. 2.2. Table 2 provides a comprehensive summary of parameters for the two sample groups.

3. Results

In this section, we investigate how the mass and orbit of the giant planet affects the formation of terrestrial planets. Our model allows for the possibility of planetesimals and planetary embryos colliding with the outer gas giant and recording changes to its

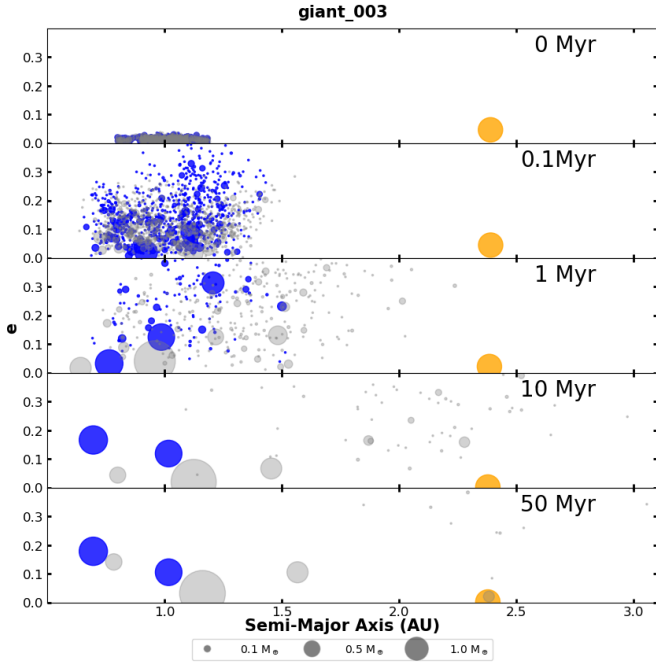


Fig. 2. Snapshots of terrestrial planet evolution. The orange dot denotes a gas giant with a mass of $1.0 M_{\text{Jup}}$. The blue dots trace the evolution of planetesimals and planetary embryos. Grey dots are used as a background to illustrate the evolutionary paths of terrestrial planets in the absence of a gas giant’s perturbation.

mass. However, the outer gas giant is more likely to eject planetary embryos from the system due to the gravitational slingshot effect. We present our main findings in Sect. 3.1. Subsequently, we describe the concept of gap complexity, C , from Gilbert & Fabrycky (2020) and followed the approach in He & Weiss (2023) to analyze our simulation results in Sect. 3.2. Finally, we conducted a statistical analysis of the simulation samples, with the results shown in Sect. 3.3.

3.1. Effect of gas giants

In Fig. 2, we show snapshots of giant_003, where a giant is placed (represented by an orange dot) at 2.4 AU with a mass of $1.0 M_{\text{Jup}}$. We used grey dots as a background to illustrate the evolution of terrestrial planets in the absence of a gas giant’s perturbation. The blue dots indicate masses, orbits and eccentricities of planetesimals and planetary embryos. The results show that the eccentricity of the particles increases significantly in the early stages of evolution, which promotes orbital crossing and collisions among the particles. Compared with scenarios lacking an outer giant, the planetary system stabilizes quickly at 10 Myr, with most of the inner mass being ejected from the system by the giant. Additionally, the orbit of the giant is affected by the inner disk, leading to a gradual decrease in its eccentricity. In the end, the two remaining planets, which have a mass similar to that of Earth, maintain a high eccentricity because their orbits are close to each other. Under the influence of their gravitational forces, the eccentricity remains between 0.1 and 0.2. We further discuss the eccentricity variations across different models in Sect. 3.3.

The results of the samples, giant_001-020 and nogiant_000, are presented in Fig. 3. The plot shows the result of the planetary system simulations after a time of approximately 50 Myr. By this stage, only a few massive particles remain, forming the final

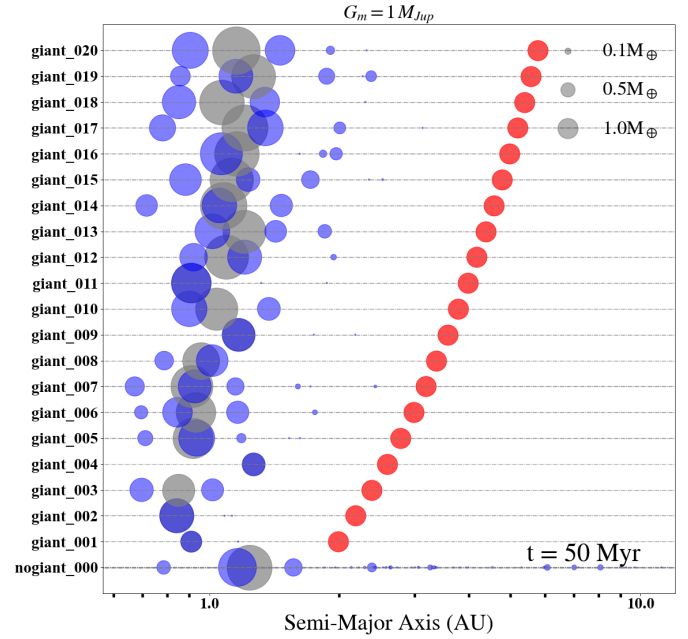


Fig. 3. Planetary system after approximately 50 Myr, illustrating the effect of placing a Jupiter-mass giant planet (indicated by red dots). The blue dots represent terrestrial planets, with the scale provided in the upper right corner. The position of each red dot indicates the location of the outer gas giant planet. In this plot, the mass of the giant is fixed at $1 M_{\text{Jup}}$. The position of the gray dot reflects the weighted average radius of the terrestrial planets (blue dots), and the size of the gray dot signifies the total mass of these terrestrial planets. It is important to note that a mass threshold of $\geq 0.1 M_{\oplus}$ is applied in the calculation of the gray dot.

architecture of the planetary system (Levison & Agnor 2003; Raymond et al. 2004, 2006a). The position of the gray dot gives the weighted average radius of the blue dots, while the size of the gray dot represents the sum of the masses of the blue dots. We note that there is a mass cut, $\geq 0.1 M_{\oplus}$, applied when calculating the gray dot to exclude the influence of any remaining low-mass particles. In addition, there is no giant in the sample nogiant_000, as shown in the bottom row of Fig. 3. By comparing nogiant_000 with giant_001-020, it becomes evident that the presence of an exterior gas giant leads to a more compact orbital configuration for the inner terrestrial planets. The presence of a giant relatively close to the planetesimal disk suppresses the growth of the terrestrial planets and pushes their location closer to the star. Moving the giant further away from the planetesimal disk, on the other hand, will increase the diversity of terrestrial planets. The gray dots indicate that as the gas giant moves away from the planetesimal disk, there is a gradual increase in both the total mass of the remaining planets within the system and their mean orbital radius.

It is necessary to study the statistical properties of N -body simulation, due to the chaotic nature of their evolution (Kokubo et al. 2006). Consequently, we have set up an additional set of samples, clone_001-020, to investigate the impact of initial states of planetesimals and planetary embryos on formation outcomes, as depicted in Fig. 4, while maintaining unchanged conditions for the outer gas giant. The findings demonstrate that random perturbations in the initial state of planetesimals and planetary embryos exert significant influences on the orbits and masses of the resultant terrestrial planets, as evidenced by the distribution pattern depicted by blue dots in the illustration. However, the initial conditions of planetesimals and planetary embryos seem

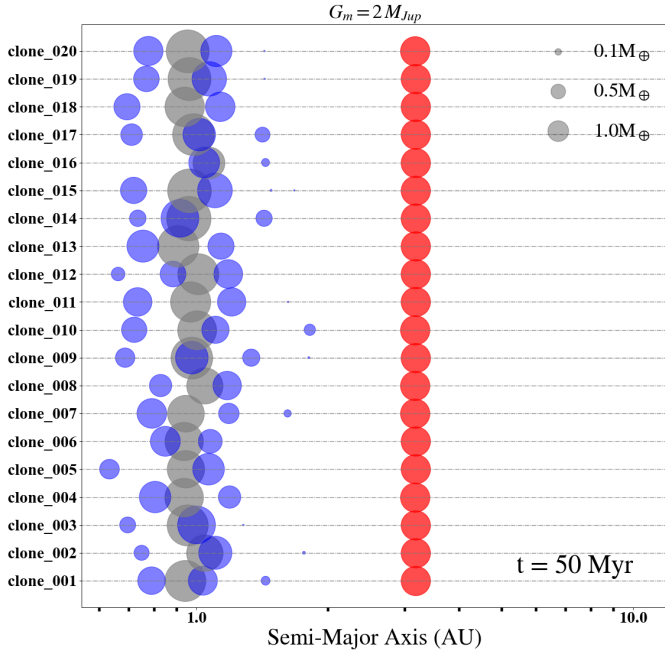


Fig. 4. The clone_001-020, which assumes the same initial state of a gas giant and randomly generates planetesimals and embryos based on their distribution, as discussed in Sect. 2.2. We find that slight differences in the initial state of planetesimals and embryos significantly impact on the resulting planetary systems (indicated by blue dots). However, this influence can be reduced by considering the mean orbit of the planets (represented by gray dots).

to have little effect on the final total mass and mean orbit of the inner terrestrial planets, as shown in the distribution of gray dots in the figure. Therefore, the total mass and mean orbital characteristics of the inner remnant terrestrial planets in a planetary system can serve as robust physical parameters for investigating the formation process of such planets, thereby mitigating the influence of initial conditions pertaining to planetesimals and planetary embryos on the obtained results.

For models that do not contain any external gas giant, we also set up random samples designated as “no giant” to study the effects of the initial state of planetesimals and planetary embryos on planet formation, as shown in Fig. 5. The findings depicted in the figure are consistent with those illustrated in Fig. 4, where random changes in the initial state of planetesimals and planetary embryos have a significant impact on the results. Again, this effect can be significantly reduced by considering instead the total mass and mean orbit of the planets. By comparing Figs. 3 and 5, it is further emphasized that the inclusion of outer gas giants would result in a more tightly confined orbit for the terrestrial planet formed within its inner boundary.

Next, we concentrate the results of the “with giant” group in Fig. 6. The x coordinate is the position of the initial gas giant planet, and the y coordinate shows the total mass of all remaining inner terrestrial planets, with $m \geq 0.1 M_{\oplus}$, in the system. The simulated samples of various gas giant states are represented by dots in different colors. Moreover, polynomials were utilized to individually fit points of the same color, enhancing the clarity of data trends. The next series of plots use the same legend. To enhance the visibility of the outcome, we use dotted lines in corresponding colors to fit the data points in Fig. 6. There is a clear trend that the total mass of the remaining terrestrial planets increases as the gas giants move away from the inner planetesimals. There

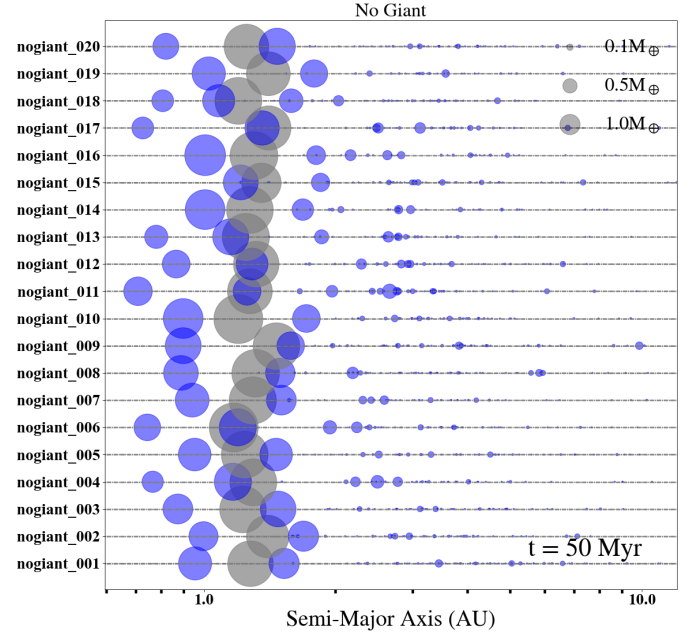


Fig. 5. No giant samples, with the initial states of planetesimals and planetary embryos randomly generated based on their distribution. The findings depicted in the figure are consistent with the points made in Fig. 4, namely, that the total mass and mean position of the formed planets is relatively constant despite the variation in the detailed planetary architectures. Moreover, this plot further underscores that including an outer gas giant leads to a more tightly confined orbit for terrestrial planets formed within its inner boundary, compared with Fig. 3.

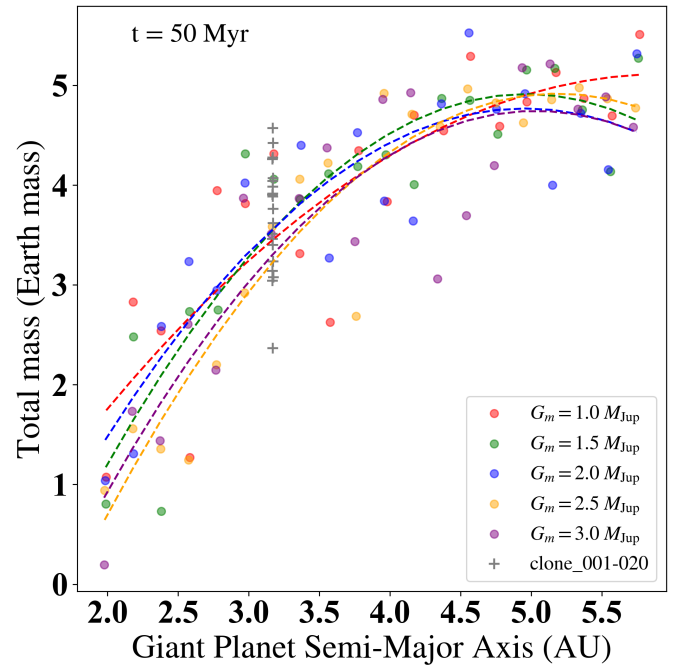


Fig. 6. Total mass in terrestrial planets at the end of the simulation, as a function of the semi-major axis of the gas giant. The different colored dots represent the effect of different gas giant masses on the simulation results. The plus dots represent the clone_001-020 with the gas giant at 3.2 AU. There is a clear trend (indicated by a dashed line representing a second order polynomial fit) that the total mass of the remaining terrestrial planets increases as the gas giants move away from the inner planetesimals.

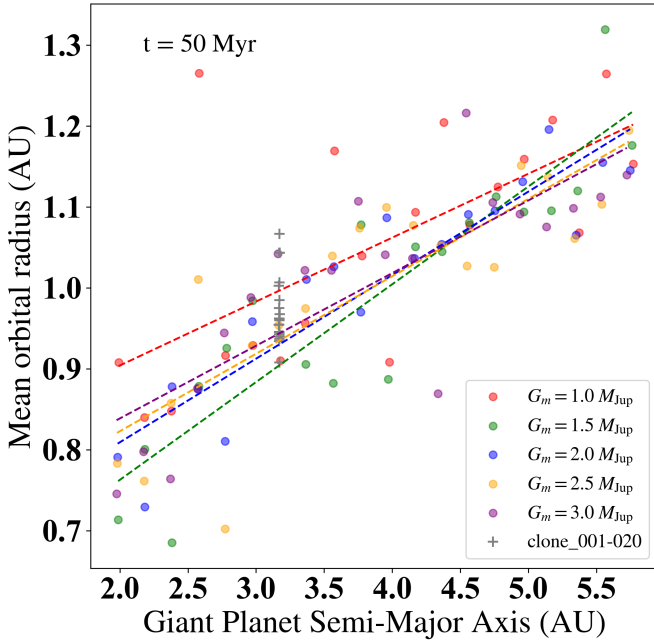


Fig. 7. Mean orbital radius as a function of the semi-major axis of the giant planets. There is a clear trend (indicated by a dashed line representing a linear fit) that the weighted average of the orbits of the inner terrestrial planets increases as the gas giant moves away from the inner planetesimals.

is also a weak tendency for the corresponding fitting curve to move downward overall as the mass of the gas giant increases. These phenomena can be attributed to the gravitational interaction between the gas giant and the planetesimal disk. When the gas giant is close to the planetesimal disk, consequently, certain planetesimals and planetary embryos are either captured by or ejected from the system due to their attraction towards the gas giant, resulting in a reduction in mass for the remaining terrestrial planets. As the gas giant moves away from the planetesimal disk, its gravitational influence weakens, leading to an increased mass and orbital diversity among the inner terrestrial planets. Similarly, as the mass of the gas giant increases, its gravitational influence increases and the fitting curve moves downward. Furthermore, the distribution of these samples (clone_001-020) does not exhibit a distinct segregation from the overall distribution of the samples (giant_001-100), implying that the initial state of planetesimals and planetary embryos less influence on the mass of the remaining terrestrial planets.

In Fig. 7, we replace the y-coordinate with the weighted average of the orbits of the inner terrestrial planets, defined as $m \geq 0.1 M_{\oplus}$. There is a clear trend that the weighted average of the orbits of the inner terrestrial planets increases as the gas giant moves away from the inner planetesimals. Meanwhile, the fitted curve drifts downward as the mass of the initial gas giant increases. This also implies that as gas giants decrease in mass or move further away from planetesimals, their gravitational influence on the planetary disk weakens, resulting in an expanded orbital distribution of the formed terrestrial planets. The distribution of the samples, clone_001-020, exhibits a greater concentration in Fig. 7, compared to Fig. 6, implying that the initial states of planetesimals and planetary embryos exert a diminished influence on the average orbital characteristics of terrestrial planets when compared to the total mass.

Finally, Fig. 8 displays the total mass as a function of the mean orbit for all simulation samples. In this figure, we use black

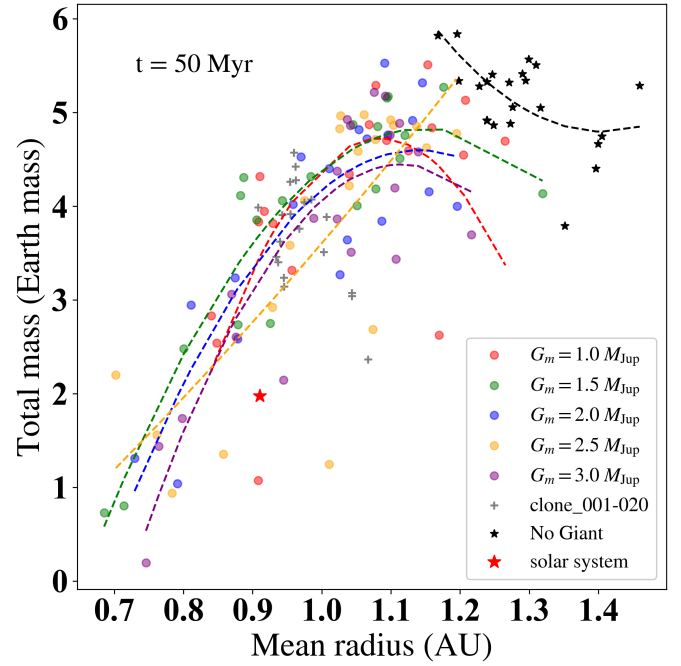


Fig. 8. Total mass of terrestrial planets as a function of the mean orbit for all simulation samples. The black stars represent the “no giant” group and the red star represents the Solar System. The figure indicates that simulations setups containing a gas giant and those without gas giants fall into two distinct groups.

stars to represent the “no giant” group and red star represents the Solar System. The figure shows that samples containing gas giants designated as “with giant” and the samples marked “no giant” are divided into two distinct groups. Due to the gravitational influence of the outer gas giant, the inner terrestrial planets exhibit relatively low residual mass and mean orbital radius. As the gas giant gradually moves away from the planetesimal disk, its gravitational impact weakens, leading to an increase in both mass and orbital width of these inner terrestrial planets. For the simulations related to “no giant” located in the upper-right corner of the image, the terrestrial planets formed without the influence of an outer gas giant, resulting in more widely dispersed orbits and a greater residual mass.

3.2. Gap complexity

A previous study by He & Weiss (2023) used the catalog from the *Kepler* Giant Planet Search (KGPS) to study the relation between inner planets with the outer giant, and they used the gap complexity, C , to describe this orbital diversity (Gilbert & Fabrycky 2020). The gap complexity is defined as:

$$C \equiv -K \left(\sum_{i=1}^n p_i^* \log p_i^* \right) \cdot \left(\sum_{i=1}^n \left(p_i^* - \frac{1}{n} \right)^2 \right). \quad (1)$$

Here, n is the number of adjacent planet pairs (i.e. gaps) in the system, therefore at least three planets are required to compute the C . Also, K is a multiplicity-dependent normalization constant chosen such that C is always in the range (0, 1). The exact value of K needs to be calculated according to Anteneodo & Plastino (1996). Here we use the approximate value, defined as follows:

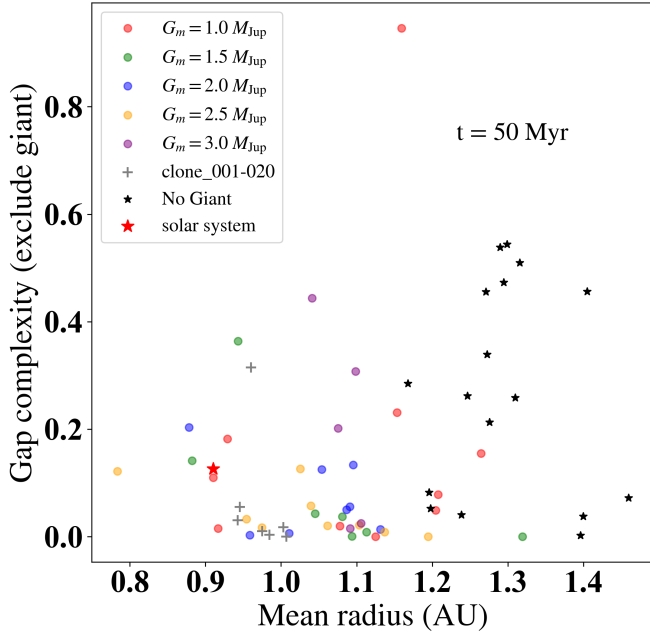


Fig. 9. Gap complexity, excluding the giant planet, as a function of the mean orbital radius of the inner planets. The black stars represent the “no giant” group and the red star represents the Solar System. The figure indicates that the gap complexity within the inner multi-planet system is relatively low due to the influence of the outer giant’s gravity.

$$K \approx \frac{1}{0.262 \ln(0.766n)}. \quad (2)$$

The quantity p_i^* represents the orbital period information of planet, as defined below:

$$p_i^* = \frac{\log \mathcal{P}_i}{\log \left(\frac{P_{\max}}{P_{\min}} \right)}. \quad (3)$$

The quantity $\mathcal{P}_i \equiv P_{i+1}/P_i$ denotes the period ratios, while P_{\min} and P_{\max} are the minimum and maximum periods in the system. The gas complexity is designed to quantify the degree of departure from perfectly regular spacings within a system, ranging from 0 (indicating evenly spaced planets in log-period) to 1 (representing maximum complexity).

He & Weiss (2023) showed that observed systems with an outer giant planet have a higher gap complexity of the inner planets. However, the computation of gap complexity, C , necessitates the presence of at least three planets within the system. Excluding the remote giant planets, only 26 planetary systems from the *Kepler* Giant Planet Search (KGPS) satisfy this criterion, featuring at least three inner planets. These systems were subsequently categorized into 22 samples without an outer gas giant and 4 samples with on outer giant. However, the limited size of the observational sample presents challenges in discerning whether structural disparities in multi-planet systems arise from physical processes or incomplete observations. Therefore, our aim was to employ simulations to investigate gap complexity as a quantitative measure of diversity within planetary systems. First, we removed particles of less than $0.1 M_{\oplus}$ and the outer giant when calculating the gap complexity, C . That minimizes the influence of low-mass particles and the outer giant in the results. We show the results in Fig. 9. In the figure, the gap complexity excluding the giant planet is shown as a function of the mean orbital radius of the inner planets. The black stars represent the “no giant”

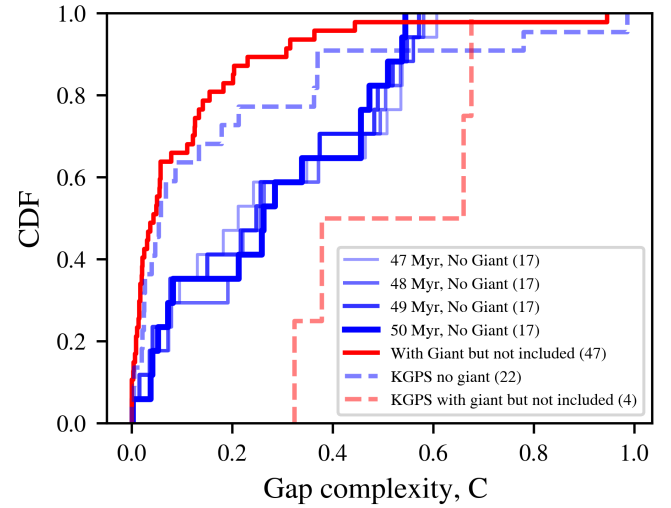


Fig. 10. Cumulative distributions of gap complexity. The blue lines represent “no giant” group, while the gradient and thickness colors are used to represent time from 47 to 50 Myr. The red line represent the “with giant” group. The blue and red dashed lines indicate the results without and with giants in the observed sample KGPS, respectively. All samples exclude giant from gap complexity calculations. The legend indicates the number of available samples in each sample set.

group and the red star represents the Solar System. However, due to the requirement to include at least three planets when calculating gap complexity, C , this leads to a reduction in the available samples. By analyzing these data we can find that the gap complexity within the inner multi-planet system is relatively low due to the influence of the outer giant’s gravity.

Next, we compared the cumulative distributions of gap complexity in our simulated samples with the KGPS samples, as shown in Fig. 10. The red line represents “with giant” group at 50 Myr. For the “no giant” group, the AMD (Angular Momentum Deficit) of the planetary system has not stabilized, as detailed in Sect. 3.3, where we use gradient and thickness of blue lines representing results from 47 to 50 Myr. However, before calculating the gap complexity, we remove particles of less than $0.1 M_{\oplus}$, therefore the evolution time has little effect on the cumulative distribution of the gap complexity. There are still significant differences between our simulated samples and the KGPS samples. For example, the trend seen among the “with giant” samples is similar to the “no giant” samples in KGPS. Here, we present two possible causes to explain the difference between simulation and observation: a) due to limitations in the observing time of *Kepler*, outer gas giants in multi-planet systems cannot be directly observed. Consequently, the KGPS no giant samples (blue dashed line) could be mixed with outer giants that are not observed. As a result, the distribution function (CDF) curve of KGPS no giant (blue dashed line) falls between the simulated samples “with giant” (red line) and “no giant” (blue line). In the simulation samples, the gravity of the outer giant influences the orbit distribution of the inner multi-planet system, resulting in a relatively uniform distribution and low gap complexity values. Furthermore, the KGPS with giant samples (red dashed line) only contain four available samples, rendering this subset of results statistically insignificant; b) in the KGPS “no giant” samples, the super-Earths may form a resonant chain during the process of pebble accretion and migration (Terquem & Papaloizou 2007; Ogiwara & Ida 2009; Cossou et al. 2014; Izidoro et al. 2017; Izidoro et al. 2021;

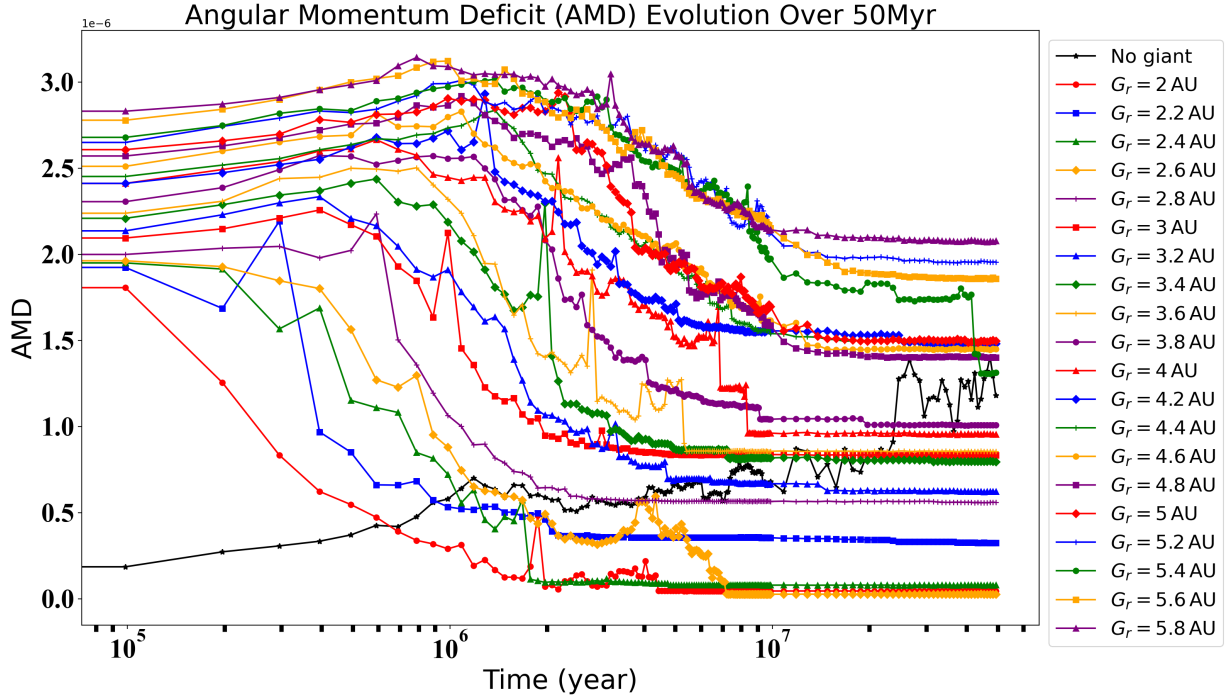


Fig. 11. Evolution of the angular momentum deficit (AMD) over 50 Myr in some samples (giant_001–020 and nogiant_000). The results indicate that the AMD represented by the black curve (No Giant) has not stabilized, whereas most of planetary systems have stabilized by 50 Myr.

Kajtazi et al. 2023), which results in a low value of the gap complexity (blue dashed line). Gravitational perturbations from the outer giants can disrupt the resonant orbits of the inner planets, leading to an increase in the gap complexity (red dashed line). However, our simulation sample adopts the classical collision formation model, which makes it unable to reproduce the results of the compact resonant chain formation pathway. To further elucidate the inconsistencies between the simulations and observations depicted in Fig. 10, future terrestrial planet formation simulations should consider incorporating pebble accretion and migration during the protoplanetary disc phase.

3.3. Statistical analysis

The concept of angular momentum deficit (AMD) plays a significant role in the formation of planetary systems (Laskar 1997, 2000; Laskar & Petit 2017). In studies of N -body dynamics simulations, collisions cease when the total AMD is insufficient to promote further planetary collisions. Therefore, we can use the total AMD to determine the evolution of planetary systems. In general, the total AMD is defined as follows:

$$\text{AMD} = \sum_i \lambda_i \left(1 - \sqrt{1 - e_i^2} \cdot \cos(i_i) \right), \quad (4)$$

where the sum is over all planets in the system, λ_i is the orbital angular momentum for the i th planet, e_i represents the eccentricity of the i th planet, and i_i indicates the inclination of the i th planet's orbit relative to a reference plane. In Fig. 11, we display the evolution of the angular momentum deficit (AMD) over 50 Myr in some samples (giant_001-020 and nogiant_000). The results indicate that the AMD represented by the black curve (no giant) has not stabilized, whereas most of planetary systems have stabilized by 50 Myr. Even for those samples (no giant) that are unstable, Fig. 10 shows little effect on the main results of this work. Here, we incorporated the outer gas giant into the AMD

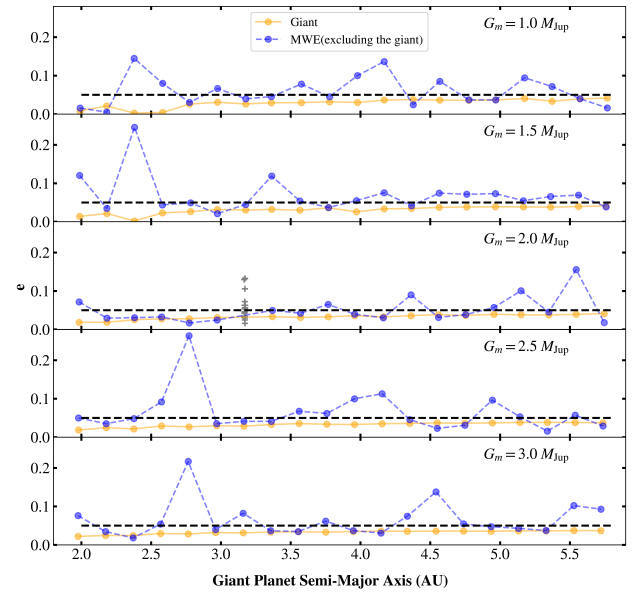


Fig. 12. Eccentricity of the “with giant” group at 50 Myr. The black dashed line represents the initial eccentricity of the giant, set at 0.05, while the orange dots depict the final giant eccentricity. The blue dots represent the mass weighted eccentricity, excluding the giant. The gray crosses represent the mass weighted eccentricity, excluding the giant, for the clone_001-020.

calculation. The eccentricity of this giant is influenced by the inner disk during the evolutionary process (seeing Fig. 2), leading to a gradual increase in the AMD value with the distance of the giant from the inner disk. This phenomenon is explained in more detail in Fig. 12.

Next, we used the mass weighted eccentricity (MWE) from Raymond et al. (2006a) to calculate the eccentricities of the

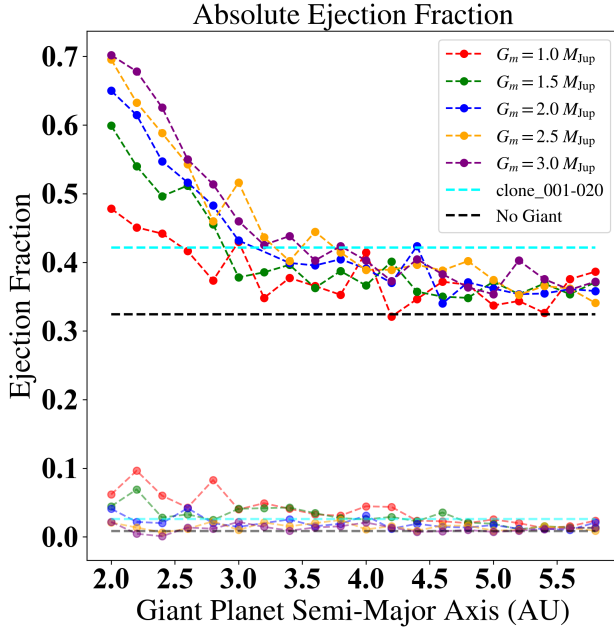


Fig. 13. Fraction of particles that are ejected from the system across all samples. The curves on the top represent the fraction of collisions with the central star (<0.2 AU). The curves at the bottom represent the ejection fraction beyond the outer boundary (>50 AU) of the system. The results indicate that the outer giant can significantly increase the particle ejection fraction.

remaining particles at 50 Myr for all samples containing giants, as illustrated in Fig. 12. The mass weighted eccentricity (MWE) is defined as follows:

$$\text{MWE} = \frac{\sum_j m_j e_j}{\sum_j m_j}, \quad (5)$$

where we sum over all surviving bodies j (excluding the giant). In Fig. 12, the black dashed line represents the initial eccentricity of the giant, set at 0.05, while the orange dots represent the final eccentricity of giant. The trend depicted by the orange curve indicates that as the orbital radius of the giant increases, its eccentricity is less affected by the inner disk. This results in a smaller deviation between the final eccentricity and the initial preset eccentricity. This trend, where the eccentricity of the giant planet increases with the increase of its orbital radius, is also reflected in Fig. 11 during the calculation of the angular momentum deficit (AMD), which shows that the AMD increases as the giant planet’s orbit becomes more distant. The blue dots represent the mass weighted eccentricity (MWE), excluding the giant. The peaks observed here signify that these samples possess a high eccentricity and the influence of orbital resonance can be ruled out based on our orbital parameters. While the gray crosses suggest that the initial state of planetesimals and planetary embryos influences the final system’s eccentricity, this deviation alone is insufficient to account for all the observed peaks. In fact, the snapshot depicting the evolution of the terrestrial planets presented in Fig. 2 corresponds to the first peak in the upper left corner of Fig. 12. Consequently, the multiple terrestrial planets that ultimately form on the inner side are likely to increase the system’s mass weighted eccentricity (MWE) due to gravitational interactions, leading to the observed peaks.

Subsequently, in Fig. 13, we show the fraction of particles that are ejected from the system across all samples. The curves at the top represent the fraction of collisions with the central star

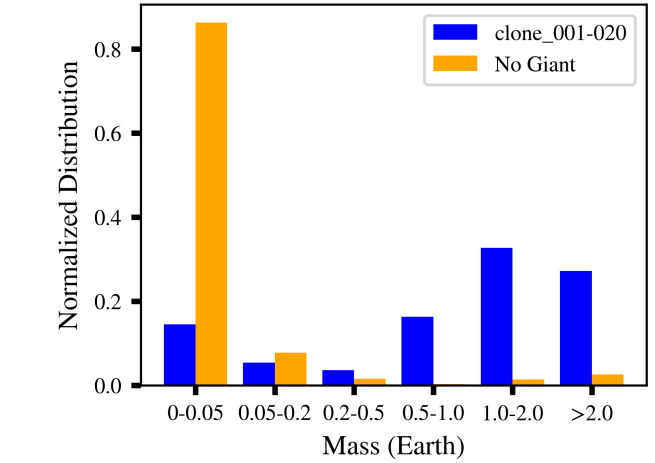


Fig. 14. Statistical histogram depicting the mass distribution of terrestrial planets and remaining planetesimals. The blue bars represent the clone_001-020, which includes a giant planet fixed at 3.2 AU, while the orange bars represent the “no giant” group. This suggests that the gravitational influence of an outer gas giant actually facilitates the formation of massive terrestrial planets by affecting the interactions between planetesimals and planetary embryos in the terrestrial planet zone.

(<0.2 AU). The curves at the bottom represent the ejection fraction beyond the outer boundary (>50 AU) of the system. Comparing the black dashed line (no giant) to the colored dashed lines (with giant), the results indicate that the outer giant can significantly increase the particle ejection fraction. On the left side of Fig. 13, the gravitational impact on the inner disk intensifies with the increasing mass of the giant, leading to a higher fraction of particles deviating from their original orbits and either colliding with the central star or being ejected from the system. Given that the gravitational force diminishes with the square of distance, the radius of the giant’s orbit exerts a negligible influence on the ejection ratio of the inner particles beyond approximately 5 AU. In the “no giant” group, approximately 22.9% of the particles experienced planetesimal-to-planetesimal collisions before crashing into the central star. Therefore, in the model with fully active particles, collisions between planetesimals may increase the proportion of particles deviating from their original orbits and crashing into the central star (<0.2 AU), even without the influence of the outer giant. In addition, upon comparing Figs. 12 and 13, we find a strong correlation between the decrease in giant eccentricity and the mass of the ejected planetesimals and embryos from the system. As the giant orbits closer to the inner planetary disk, more mass is ejected from the system (<0.2 AU or >50 AU), resulting in a decrease in the eccentricity of the giant.

Next, we show a statistical histogram of different masses of the terrestrial planets and remnant planetesimals in Figs. 14 and 15. The particles that have not gained significant mass (initial planetesimals and embryos) are indicated in column 0–0.05 M_{\oplus} . In Fig. 14, the blue bars represent the samples of the clone_001-020, $G_m = 2.0 M_{\text{Jup}}$ and $G_a = 3.2$ AU and the orange bars represent the “no giant” samples. The findings reveal that when there is no gas giant in an exterior orbit (orange data), most particles fail to undergo mass growth through mutual collisions, and even a minimal increase in mass does not lead to the formation of a massive planet. However, the presence of an exterior gas giant (blue data) leads to a higher number of particles involved in the collision process, resulting in the formation of massive planets. This suggests that the gravitational influence

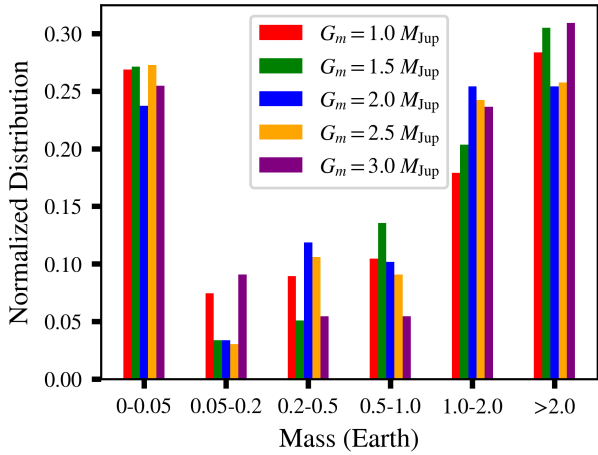


Fig. 15. Statistical histogram depicting the mass distribution of terrestrial planets and the remaining planetesimals. We have categorized the samples into five groups based on the initial mass of the giants, each represented by a distinct color. Comparing with the “no giant” in Fig. 14, the result shows that the presence of more massive gas giants in the outer region of the planetesimal disk significantly increase the likelihood of forming massive terrestrial planets in the inner regions.

of the outer gas giants facilitates the formation of massive terrestrial planets through their impact on the interaction between planetesimals and planetary embryos within planetesimals.

In Fig. 15, we show a statistical histogram of different mass sizes of the terrestrial planets and remnant planetesimals in the “with giant” sample and we divided the sample into five categories based on the mass of the giant planet, represented by different colors. However, there are no significant differences in the distribution patterns of these five categories. With the increase in the mass of the giant, there is only a slight decrease in the proportion of planets in the 0.5–1.0 M_{\oplus} range and a slight increase in the proportion of planets in the 1.0–2.0 M_{\oplus} range. The figure shows that when the planetary system evolves to a time of 50 Myr, only about 25% of planetesimals remain with a mass below 0.05 M_{\oplus} , which means that the mass of these particles have not increased significantly. Comparing with the “no giant” group in Fig. 14, the result shows that the presence of gas giants in the outer region of the planetesimal disk enhances the likelihood of forming massive terrestrial planets on the inside.

Finally, we show a cumulative distribution of both minor and major planetary bodies that formed, using all the samples we studied, in Fig. 16. We use different colors representing different sample sets. The curves in the figure are categorized into three groups based on different sample sets. The black curve at the top represents samples of “no giant” and the bottom cyan curve represents samples of the different initial states of the planetesimals and planetary embryos clone_001-020, with the middle samples (giant_001-100) divided into five different curves, depending on the mass of the initial gas giant. The results here are consistent with Figs. 14 and 15 showing that gas giants on the outside of the planetesimals disk facilitates the formation of massive terrestrial planets on the inside.

4. Conclusions

Here, we present a comprehensive summary of the simulation results for two distinct types of samples. We investigated the influence of outer gas giants on the formation of a system of terrestrial planets in giant_001-100. We took the same initial state of a gas giant as giant_047 and randomly generated

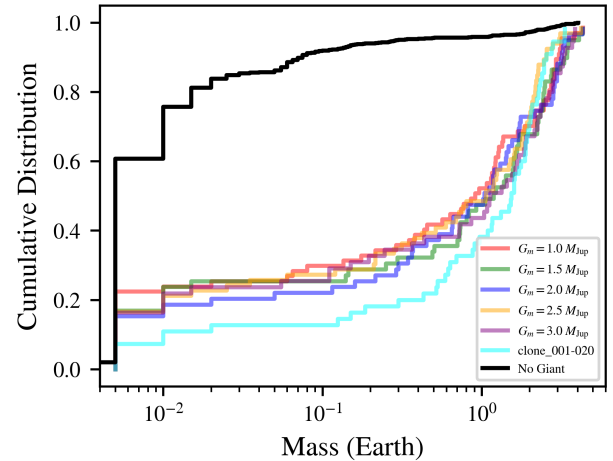


Fig. 16. Cumulative distribution of both minor and major planetary bodies that formed in our simulations, with different colors representing distinct sample sets.

planetesimals and embryos in clone_001-020. We represented scenarios where only planetesimals and embryos are present, without a gas giant. We outline the limitations of our model below and provide a forward-looking perspective on avenues for future research endeavors.

4.1. Summary of our simulation results

1. With giant: in Fig. 3, we show the results of planetary system simulation of approximately 50 Myr. By this stage, only a few massive particles remain, forming the final architecture of the planetary system (Levison & Agnor 2003; Raymond et al. 2004, 2006a). By comparing the samples nogiant_000 and giant_001-100, it becomes evident that the presence of an outer giant leads to more compact orbital configuration for the inner terrestrial planets. Meanwhile, a gas giant too close to the planetesimal disk entirely prevents the formation of terrestrial planets. Also, the number and size of the remaining planets in planetary systems are relatively limited for a close-in giant planet. Moving the gas giant further away from the planetesimal disk will increase the diversity of terrestrial planetary. Meanwhile, we show the evolution of the angular momentum deficit (AMD) over 50 Myr in some samples (giant_001-020) in Fig. 11. The results indicate that the AMD represented by the “no giant” sample has not stabilized, whereas most of planetary systems have stabilized by 50 Myr. While keeping the conditions of the outer gas giant constant (clone_001-020), the findings demonstrate that random perturbations to the initial state of planetesimals and planetary embryos exert significant influences on the orbits and masses of the resultant terrestrial planets. However, the initial conditions of planetesimals and planetary embryos seems to have little effect on their final total mass and mean orbit of the inner terrestrial planets in Fig. 4. Therefore, the total mass and mean orbital characteristics of the inner remnant terrestrial planets in a planetary system can serve as robust physical parameters for investigating the formation processes of such planets.
2. No giant: For models that do not harbour an outer gas giant, our findings are consistent with the fixed-giant samples, represented in clone_001-020, where small changes in the initial state of planetesimals and planetary embryos have a significant impact on the results (as shown in Fig. 5). Furthermore,

this effect can be significantly reduced by calculating the total mass and mean orbit of the remaining planet.

3. Effect of gas giants: Under the gravitational influence of a outer giants, collisions between inner planetesimals and embryos are promoted, which accelerates the formation process of terrestrial planets (Fig. 11) while also ejecting a large number of particles out of the planetary system (Fig. 13). Therefore, when the giant is close to the inner disk, the total mass and mean orbital radius of the ultimately formed terrestrial planets are smaller. When the giant is moved away from the inner disk to a distance of 5 AU, due to the weakened gravitational influence of the giants, the total mass and mean orbital radius of the resulting terrestrial planets becomes greater (Fig. 3). Moreover, the orbit of the giant itself is modulated by the gravitational pull from the inner disk, resulting in a gradual reduction in the eccentricity of the giant's orbit in Fig. 2. However, this modulatory effect diminishes as the orbital radius of the giant extends away from the inner disk in Fig. 12 (Levison & Agnor 2003; Raymond et al. 2006a). In addition, upon comparing Figs. 12 and 13, we find a strong correlation between the decrease in giant eccentricity and the mass of the ejected planetesimals and embryos from the system. As the giant orbits closer to the inner planetary disk, more mass is ejected from the system (<0.2 AU or >50 AU), resulting in a decrease in the eccentricity of the giant.
4. Gap complexity: Under the classical theory, where planetary embryos and planetesimals collide to form terrestrial planets, our simulation results do not reach the same conclusion as He & Weiss (2023) that the presence of an outer giant increases the gap complexity of the planetary system. In contrast, our results show that the presence of a giant planet actually decreases the gap complexity. We believe that this difference between these two results may arise due to different planet formation scenarios. The systems of super-Earths and mini-Neptunes analyzed by He & Weiss (2023) were likely formed within the protoplanetary disc and experienced significant migration and subsequent planetary instabilities (Lambrechts et al. 2019; Izidoro et al. 2021; Kajtazi et al. 2023). The classical terrestrial planet formation simulations employed here, on the other hand, yield smaller planets that are not subject to disk migration, due to their formation after the dissipation of the protoplanetary disk.
5. Statistical analysis: The implication of this analysis is that when the gas giant is close to the planetesimal disk, its gravitational influence is amplified and this expedites the collision or scattering of planetesimals and planetary embryos, resulting in a rapid reduction in the number of particles in the system. When the gas giant is moved away from the planetesimal disk, its gravitational influence weakens, resulting in reduced collisions between planetesimals and planetary embryos. Moreover, Figs. 14–16 show that a gas giant on the outside of the planetesimal disk facilitates the formation of massive terrestrial planets on the inside. However, if the giants are too close to the disk of planetesimals and embryos, this would prevent the formation of large-sized terrestrial planets (see Fig. 3).

4.2. Future research

In our study, the cost of our N -body simulation model imposes stringent constraints on the possibility to vary our initial parameters of inner planetesimals and planetary embryos. Specifically, in giant_001-100, we chose to keep the initial conditions for planetesimals and planetary embryos identical. As a result, our

conclusions are subject to the limitation that we did not explore a wider range of initial conditions for planetesimals and planetary embryos. In nogiant_000-020 and clone_001-020, we nevertheless briefly explore the impact of randomized variations in the initial positions of inner planetesimals and planetary embryos on the simulation results. These changes are seen to have an impact on the specific outcome of the simulations, but not on averaged properties, such as mean mass and position. In addition, the narrow model we use, which concentrates planetesimals and planetary embryos around 1 AU in the initial conditions, makes it difficult for us to discuss the sources of water in planets and the relationship between different gas giant orbits and planet formation in the habitable zone, compared to the wide condition (Raymond 2006; Ronco & de Elía 2018; Zain et al. 2018). Furthermore, any consideration of the migration of the gas giant was omitted in our study. Previous research has demonstrated that the migration and instability of gas giants can significantly influence the dynamics of inner planets (Fogg & Nelson 2005, 2007; Raymond et al. 2006b; Thommes et al. 2008; Nesvorný et al. 2021). We note that we also ignored the growth of the embryos by pebble accretion. Thus, incorporating other accretion mechanisms and various gas giant migration models will be a focal point of our future investigations.

Acknowledgements. We would like to thank the referee, Sean Raymond, for many comments that helped improve the manuscript. Z.K. thanks the support by the National Natural Science Foundation of China under Grants Nos. 11920101003, 12021003, and 11633001, and the Strategic Priority Research Program of Chinese Academy of Sciences, Grant No.XDB23000000. A.J. acknowledges funding from the Danish National Research Foundation (DNRF Chair Grant DNRF159), the Carlsberg Foundation (Semper Ardens: Advance grant FIRSTATMO), the Knut and Alice Wallenberg Foundation (Wallenberg Scholar Grant 2019.0442) and the Göran Gustafsson Foundation. M.L. acknowledges funding from the European Research Council (ERC Starting Grant 101041466-EXODOSS). J.H.J. acknowledges the support by the Jet Propulsion Laboratory, California Institute of Technology, sponsored by NASA. The Tycho supercomputer hosted at the SCIENCE HPC center at the University of Copenhagen was used for supporting this work.

References

- Anteneodo, C., & Plastino, A. 1996, *Phys. Lett. A*, 223, 348
- Batygin, K., & Morbidelli, A. 2023, *Nat. Astron.*, 7, 330
- Brasser, R., Matsumura, S., Ida, S., Mojzsis, S. J., & Werner, S. C. 2016, *ApJ*, 821, 75
- Brasser, R., Grimm, S. L., Hatalova, P., & Stadel, J. G. 2023, *A&A*, 678, A73
- Briceño, C., Vivas, A. K., Calvet, N., et al. 2001, *Science*, 291, 93
- Brož, M., Marchis, F., Jorda, L., et al. 2021, *A&A*, 653, A56
- Carrera, D., Johansen, A., & Davies, M. B. 2015, *A&A*, 579, A43
- Chambers, J. E. 1999, *MNRAS*, 304, 793
- Chambers, J. 2001, *Icarus*, 152, 205
- Chambers, J., & Wetherill, G. 1998, *Icarus*, 136, 304
- Clement, M. S., Kaib, N. A., Raymond, S. N., & Walsh, K. J. 2018, *Icarus*, 311, 340
- Clement, M. S., Raymond, S. N., & Kaib, N. A. 2019, *AJ*, 157, 38
- Cossou, C., Raymond, S. N., Hersant, F., & Pierens, A. 2014, *A&A*, 569, A56
- Everhart, E. 1985, in *Astrophysics and Space Science Library*, 115, IAU Colloq. 83: Dynamics of Comets: Their Origin and Evolution, eds. A. Carusi, & G. B. Valsecchi, 185
- Fogg, M. J., & Nelson, R. P. 2005, *A&A*, 441, 791
- Fogg, M. J., & Nelson, R. P. 2007, *A&A*, 472, 1003
- Gilbert, G. J., & Fabrycky, D. C. 2020, *AJ*, 159, 281
- Grimm, S. L., & Stadel, J. G. 2014, *ApJ*, 796, 23
- Guo, K., & Kokubo, E. 2023, *ApJ*, 955, 109
- Haisch, Karl E., J., Lada, E. A., & Lada, C. J. 2001, *ApJ*, 553, L153
- Hansen, B. M. S. 2009, *ApJ*, 703, 1131
- Hasegawa, Y., & Pudritz, R. E. 2012, *ApJ*, 760, 117
- He, M. Y., & Weiss, L. M. 2023, *AJ*, 166, 36
- Hillenbrand, L. A., Carpenter, J. M., Kim, J. S., et al. 2008, *ApJ*, 677, 630
- Izidoro, A., Ogihara, M., Raymond, S. N., et al. 2017, *MNRAS*, 470, 1750
- Izidoro, A., Bitsch, B., Raymond, S. N., et al. 2021, *A&A*, 650, A152
- Izidoro, A., Dasgupta, R., Raymond, S. N., et al. 2021, *Nat. Astron.*, 6, 357

- Jacobson, S., & Morbidelli, A. 2014, *Philos. Trans. Ser. A, Math. Phys. Eng. Sci.*, **372**
- Johansen, A., Low, M.-M. M., Lacerda, P., & Bizzarro, M. 2015, *Sci. Adv.*, **1**, e1500109
- Johansen, A., Ronnet, T., Bizzarro, M., et al. 2021, *Sci. Adv.*, **7**, eabc0444
- John, F. R., Thorsten, K., & Bourdon, B. 2010, *Nat. Geosci.*, **3**, 439
- Joiret, S., Raymond, S. N., Avicé, G., et al. 2023, *Icarus*, **406**, 115754
- Kaib, N. A., & Cowan, N. B. 2015, *Icarus*, **252**, 161
- Kajtazi, K., Petit, A. C., & Johansen, A. 2023, *A&A*, **669**, A44
- Kokubo, E., Kominami, J., & Ida, S. 2006, *ApJ*, **642**, 1131
- Kong, Z., Jiang, J. H., Burn, R., Fahy, K. A., & Zhu, Z.-H. 2022, *ApJ*, **929**, 187
- Lam, C., & Kipping, D. 2018, *MNRAS*, **476**, 5692
- Lambrechts, M., Morbidelli, A., Jacobson, S. A., et al. 2019, *A&A*, **627**, A83
- Laskar, J. 1997, *A&A*, **317**, L75
- Laskar, J. 2000, *Phys. Rev. Lett.*, **84**, 3240
- Laskar, J., & Petit, A. C. 2017, *A&A*, **605**, A72
- Levison, H. F., & Agnor, C. 2003, *AJ*, **125**, 2692
- Levison, H. F., Thommes, E., & Duncan, M. J. 2010, *AJ*, **139**, 1297
- Levison, H. F., Kretke, K. A., & Walsh, K. J. 2015, in *AAS/Division of Dynamical Astronomy Meeting*, **46**, 102.03
- Lissauer, J. J., Ragozzine, D., Fabrycky, D. C., et al. 2011, *ApJS*, **197**, 8
- Liu, B., & Ormel, C. W. 2018, *A&A*, **615**, A138
- Morishima, R., Schmidt, M. W., Stadel, J., & Moore, B. 2008, *ApJ*, **685**, 1247
- Mordasini, C., Mollière, P., Dittkrist, K. M., Jin, S., & Alibert, Y. 2015, *Int. J. Astrobiol.*, **14**, 201
- Nesvorný, D., Roig, F. V., & Deienno, R. 2021, *AJ*, **161**, 50
- O'Brien, D. P., Morbidelli, A., & Levison, H. F. 2006, *Icarus*, **184**, 39
- Ogihara, M., & Ida, S. 2009, *ApJ*, **699**, 824
- Quintana, E. V., Barclay, T., Borucki, W. J., Rowe, J. F., & Chambers, J. E. 2016, *ApJ*, **821**, 126
- Raymond, S. N. 2006, *ApJ*, **643**, L131
- Raymond, S. N., & Izidoro, A. 2017, *Sci. Adv.*, **3**, e1701138
- Raymond, S. N., Quinn, T., & Lunine, J. I. 2004, *Icarus*, **168**, 1
- Raymond, S. N., Quinn, T., & Lunine, J. I. 2006a, *Icarus*, **183**, 265
- Raymond, S. N., Mandell, A. M., & Sigurdsson, S. 2006b, *Science*, **313**, 1413
- Raymond, S. N., Armitage, P. J., Moro-Martín, A., et al. 2011, *A&A*, **530**, A62
- Raymond, S. N., Armitage, P. J., Moro-Martín, A., et al. 2012, *A&A*, **541**, A11
- Raymond, S. N., Kokubo, E., Morbidelli, A., Morishima, R., & Walsh, K. J. 2014, *Terrestrial Planet Formation at Home and Abroad in Protostars and Planets VI* (University of Arizona Press)
- Rein, H., & Liu, S.-F. 2012, *A&A*, **537**, A128
- Rein, H., & Spiegel, D. S. 2015, *MNRAS*, **446**, 1424
- Rein, H., Hernandez, D. M., Tamayo, D., et al. 2019, *MNRAS*, **485**, 5490
- Ronco, M. P., & de Elía, G. C. 2018, *MNRAS*, **479**, 5362
- Terquem, C., & Papaloizou, J. C. B. 2007, *ApJ*, **654**, 1110
- Thommes, E. W., Matsumura, S., & Rasio, F. A. 2008, *Science*, **321**, 814
- Walsh, K. J., & Morbidelli, A. 2011, *A&A*, **526**, A126
- Weiss, L. M., Marcy, G. W., Petigura, E. A., et al. 2018, *AJ*, **155**, 48
- Weiss, L. M., Isaacson, H., Howard, A. W., et al. 2024, *ApJS*, **270**, 8
- Wetherill, G. W. 1990, *Annu. Rev. Earth Planet. Sci.*, **18**, 205
- Winn, J. N., & Fabrycky, D. C. 2015, *ARA&A*, **53**, 409
- Woo, J., Brasser, R., Grimm, S., Timpe, M., & Stadel, J. 2022, *Icarus*, **371**, 114692
- Wurm, G. 2018, *Geosciences*, **8**, 310
- Zain, P. S., de Elía, G. C., Ronco, M. P., & Guilera, O. M. 2018, *A&A*, **609**, A76